

# Electrochemical, Spectroscopic, and Mass Spectrometric Studies of the Interaction of Silver Species with Polyamidoamine Dendrimers

Fu-Ren F. Fan, Carolyn L. Mazzitelli, Jennifer S. Brodbelt, and Allen J. Bard\*

Department of Chemistry and Biochemistry, The University of Texas at Austin, Austin, Texas 78712-0165

Electrochemical, spectroscopic, and mass spectrometric (MS) methods were used to probe the interaction (complexation) of silver ions and zerovalent silver species with polyamidoamine generation 1 amine-terminated (PAMAMG1NH<sub>2</sub>) and generation 2 hydroxy-terminated (PAMAMG2OH) dendrimers (DDMs). Stability constants ( $K_q^+$ ) and stoichiometries ( $q$ ) (i.e., the number of silver ions complexed per DDM molecule) were determined from the voltammetric data, that is, shifts in potential and changes in peak or limiting current with addition of DDM. When the mole ratio of DDM to Ag<sup>+</sup> is  $\geq 1$ , Ag<sup>+</sup> binds with PAMAMG2OH to form a dominant 1:1 complex with a  $K_1^+$  value of  $1.1 \times 10^7 \text{ M}^{-1}$ . Under similar conditions, Ag<sup>+</sup> binds with PAMAMG1NH<sub>2</sub>, yielding a 1:1 complex with  $K_1^+ = 4 \times 10^9 \text{ M}^{-1}$ , which is consistent with the finding of the MS experiments. When the mole ratio is  $< 1$ ,  $q \geq 2$ . The  $E^0$  of the Ag–PAMAMG1NH<sub>2</sub><sup>+0</sup> couple shifted to a more negative value than that of the Ag<sup>+0</sup> couple. The negative shift in the halfwave potential also suggests that DDM binds more strongly with Ag<sup>+</sup> than with zerovalent silver species. Spectroscopic results suggest that hydroxyl-terminated PAMAMG2OH favors the formation of small zerovalent silver clusters after reduction while amine-terminated PAMAMG1NH<sub>2</sub> allows for simultaneous formation of both clusters and larger nanoparticles at similar conditions. Other quantities, such as diffusion coefficients of the complexes and molar absorptivity of the Ag<sup>+</sup> DDMs, are also reported.

We describe here electrochemical (EC), spectroscopic, and mass spectrometric (MS) studies of the interaction of silver ions and zerovalent silver clusters with two dendrimers (PAMAM DDMs). We report the dependence of the EC behavior on the nature of the ligands coordinated to the metal centers and their concentrations.

The application of EC methods to the study of coordination of complexing agents to metal ions provides a useful complement to the spectroscopic and mass spectrometric techniques.<sup>1</sup> Equilibrium constants,  $K$ , for the complexation of the metal ions and

zerovalent metallic species with different complexing agents, such as PAMAM DDMs, can be obtained from shifts in the peak potential,  $E_p$ , or halfwave potential,  $E_{1/2}$ , and the number,  $q$ , of metal ions per DDM involved in binding. They can also<sup>1</sup> be obtained from the dependence of the current during reduction of the complexed ions on the effective mole ratio of metal ions to the DDM ligands added.<sup>1a</sup> The diffusion coefficient,  $D$ , and the number of electrons involved in the electron-transfer reaction,  $n$ , can also be determined by EC methods.

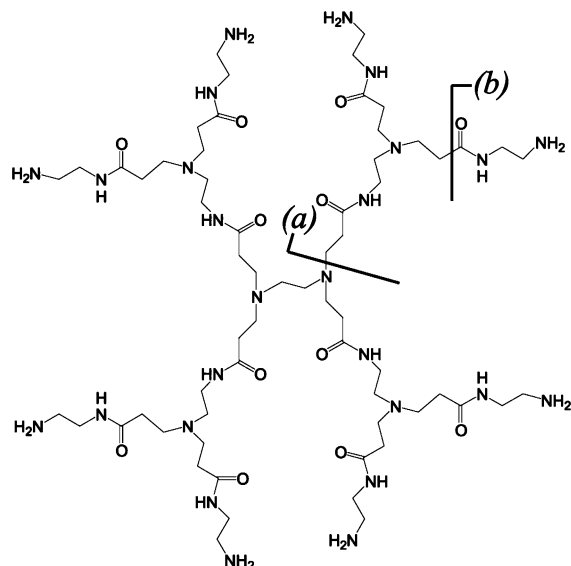
Currently, DDMs are of interest because of their unusual chemical and physical properties and also their potential applications in such diverse fields as medicine, biology, chemistry, physics, and material science.<sup>2,3</sup> For example, DDMs have served as templates for nanoparticle syntheses,<sup>4</sup> and recently, very small DDM-encapsulated silver nanodots were reported to be highly luminescent<sup>5</sup> and also show antimicrobial activity.<sup>6</sup> PAMAM can stabilize small metal clusters of defined size while the surrounding polymeric matrix protects the developing clusters against agglomeration following reduction.<sup>7</sup> By controlling the chemical structure and size of the DDMs, differently sized soluble clusters that are suitable for EC, spectroscopic, and mass spectrometric studies can be prepared. One reason for controlling the size of metal clusters or nanoparticles is to study the strong size dependence of their photochemical, electronic, and optical properties, as reported earlier by Henglein<sup>8</sup> for polyphosphate-encapsulated clusters of less than 10 silver atoms. In the present case,

- (2) (a) Newkome, G. R.; Vögtle, F. *Dendrimers and Dendrons*; Wiley-VCH: Weinheim, 2002. (b) *Dendrimers and other Dendritic Polymers*; Fréchet, J. M. J., Tomalia, D. A., Eds.; Wiley: New York, 2001.
- (3) For some recent reviews, see, for example: (a) Hecht, S.; Fréchet, J. M. J. *Angew. Chem., Int. Ed.* **2001**, *40*, 75. (b) Gorman, C. B.; Smith, J. C. *Acc. Chem. Res.* **2001**, *34*, 60. (c) Balzani, V.; Ceroni, P.; Juris, A.; Venturi, M.; Campagna, S.; Puntoriero, F.; Serroni, S. *Coord. Chem. Rev.* **2001**, *219–221*, 545. (d) Grayson, S. M.; Fréchet, J. M. J. *Chem. Rev.* **2001**, *101*, 3819. (e) Majoral, J.-P.; Caminade, A.-M.; Maraval, V. *Chem. Commun.* **2002**, 2929. (f) Diederich, F.; Felber, B. *Proc. Natl. Acad. Sci. U.S.A.* **2002**, *99*, 4778. (g) Gittins, P. J.; Twyman, L. J. *Supramol. Chem.* **2003**, *15*, 5.
- (4) (a) Crooks, R. M.; Zhao, M.; Sun, L.; Chechik, V.; Yeung, L. K. *Acc. Chem. Res.* **2001**, *34*, 181. (b) Baars, M. W. P. L.; Meijer, E. W. *Top. Curr. Chem.* **2001**, *210*, 131.
- (5) Zheng, J.; Petty, J. T.; Dickson, R. M. *J. Am. Chem. Soc.* **2003**, *125*, 7780–7781.
- (6) Balogh, L.; Swanson, D. R.; Tomalia, D. A.; Hagnauer, G. L.; McManus, A. T. *Nano Lett.* **2001**, *1*, 18–21.
- (7) Crooks, R. M.; Lemon, B. I.; Sun, L.; Yeung, L. K.; Zhao, M. Q. Dendrimer-Encapsulated Metals and Semiconductors: Synthesis, Characterization, and Applications. In *Dendrimers III: Design, Dimension Function*; Vögtle, F., Ed.; Springer-Verlag: Berlin, 2001; Vol. 212, pp 81–135.
- (8) Henglein, A. *Chem. Rev.* **1989**, *89*, 1861–1873.

\* Corresponding author. E-mail: ajbard@mail.utexas.edu.

(1) (a) Bard, A. J.; Faulkner, L. R. *Electrochemical Methods, Fundamentals and Applications*; New York: John Wiley & Sons, 2001. (b) *Determination of Stability Constants*; Rossotti, F. J. C., Rossotti, H., Eds.; McGraw-Hill: New York, 1961, Chapter 8. (c) Zhou, L.; Russell, D. H.; Zhao, M.; Crooks, R. M. *Macromolecules* **2001**, *34*, 3567.

the threshold size of a silver nanoparticle is determined by the appearance of the plasmon peak in the UV-vis spectra, as discussed below. We are particularly interested in the EC behavior of very small (a few atoms) silver clusters and their biological properties.



Structure of PAMAMG1NH<sub>2</sub> with fragments caused by defects or collisional activated dissociation labeled (a) 343.3 Da and (b) 87.1 Da.

In this paper, we describe the application of EC measurements to quantify the binding of silver ion and zerovalent silver to PAMAM DDMs. Binding is interpreted in terms of the complexation of silver species with PAMAM as the ligands. We chose to begin these investigations with the low-generation PAMAM (G1, G2) to demonstrate the feasibility, usefulness, and also the limitations of various techniques for the characterization of metal-DDM complexes and nanocomposites.

## EXPERIMENTAL SECTION

**Materials.** Amine-terminated generation 1 PAMAM (PAMAMG1NH<sub>2</sub>) and OH-terminated generation 2 PAMAM (PAMAMG2OH) dendrimers were purchased from Dendritech, Inc. (Midland, MI) or Aldrich Chemical Co. (Milwaukee, WI) and were used without further purification. Silver perchlorate (99.99% purity) and anhydrous hydrazine were purchased from Aldrich Chemical Co. and were used as received. All other chemicals were reagent grade and were used without further purification. Solutions were prepared using high-purity water ( $\rho = 18 \text{ M}\Omega\text{-cm}$ ) from a Millipore Milli-Q water purification system.

**Instrumentation and Procedures.** All EC measurements were performed with a Princeton Applied Research (PAR) model 173 potentiostat/175 universal programmer/176 current-to-voltage converter (or 179 digital coulometer) interfaced with a custom-designed data acquisition system. Ultraviolet-visible (UV-vis) spectra were obtained on a Milton Roy Spectronic 3000 Array Spectrophotometer with a 1-cm quartz cuvette. Electrospray ionization (ESI)-mass spectra were taken on a ThermoFinnigan LCQ Duo quadrupole ion trap mass spectrometer (San Jose, CA). A Harvard syringe pump (Holliston, MA) set at a flow rate of 3  $\mu\text{L}/\text{min}$  was used to directly infuse the sample solutions into the mass spectrometer. The ESI source was operated in the positive

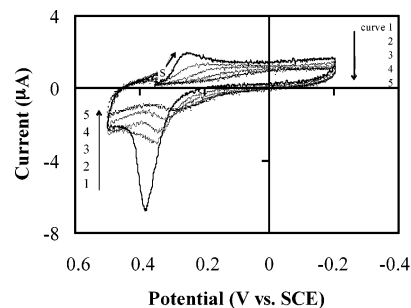


**Figure 1.** A series of cyclic voltammograms (CVs) of 0.12 mM Ag<sup>+</sup> in 0.2 M NaNO<sub>3</sub> at an inlaid Au disk electrode (radius  $\sim 0.2$  cm) in the absence and presence of various PAMAMG1NH<sub>2</sub> concentrations. Potential scan rate,  $v = 0.1$  V/s. Curve 1, no DDM; curve 2, 0.01 mM DDM; curve 3, 0.03 mM DDM; curve 4, 0.05 mM DDM; curve 5, 0.10 mM DDM. Initial potential and scan direction are labeled as S and arrow.

ion mode with an electrospray voltage of 4.0 kV and a heated capillary temperature ranging from 150 to 170  $^{\circ}\text{C}$ . Sheath and auxiliary gas flow rates of 30 and 10 arbitrary units, respectively, were used to aid in desolvation. The base pressure of the trap was  $\sim 1 \times 10^{-5}$  Torr. Spectra were acquired by summing 20 scans, each composed of 15 microscans, with an ionization time of 100 ms.

Collisional activated dissociation (CAD) experiments were performed on selected dendrimer complexes by isolating the desired precursor ion in the trap using resonance ejection, followed by increasing the collision energy applied to the trap to produce fragmentation.

All EC experiments were performed in a three-compartment cell. The working electrodes were either an inlaid Au disk (Bioanalytical Systems, West Lafayette, IN) with a geometric area of  $\sim 0.13$  cm<sup>2</sup> or an inlaid custom-made Pt disk of a geometric area of 0.008 cm<sup>2</sup>. The working electrodes were polished prior to each series of experiments with 0.25- $\mu\text{m}$  diamond paste (Buehler, Lake Bluff, IL) on a nylon cloth and then subjected to ultrasonic cleaning for  $\sim 5$  min in 95% ethanol. A saturated calomel electrode (SCE) was used as the reference electrode in all experiments. The SCE was connected to the cell through a salt bridge containing 0.2 M NaNO<sub>3</sub>, which was also used as the supporting electrolyte in all EC measurements. A Pt flag served as counter electrode. Prior to all EC measurements (unless otherwise stated), where appropriate, solutions were deoxygenated via purging with N<sub>2</sub> or Ar gas for 20–30 min. During measurements, a stream of N<sub>2</sub> or Ar was passed over the solution. Solutions for spectroscopic measurements were not deoxygenated, unless otherwise mentioned.

All experiments were carried out at ambient temperature (24.5  $\pm 0.5$   $^{\circ}\text{C}$ ).

## RESULTS

**EC Measurements. Silver-PAMAMG1NH<sub>2</sub> System, Cyclic Voltammetry.** A series of cyclic voltammograms (CVs) of 0.12 mM Ag<sup>+</sup> at an inlaid Au disk electrode (radius, 0.2 cm) in the absence and presence of various PAMAMG1NH<sub>2</sub> concentrations are shown in Figure 1. CV of Ag<sup>+</sup> at scan rate,  $v$ , of 100 mV/s, in the absence of DDM (curve 1 of Figure 1) showed reduction of Ag<sup>+</sup> to Ag<sup>0</sup> at a cathodic peak potential,  $E_{\text{pc}}$ , of +0.255 V (or halfwave potential,  $E_{1/2}^{\text{c}}$ , of +0.298 V) vs SCE. In this system, Ag<sup>0</sup> deposits on the

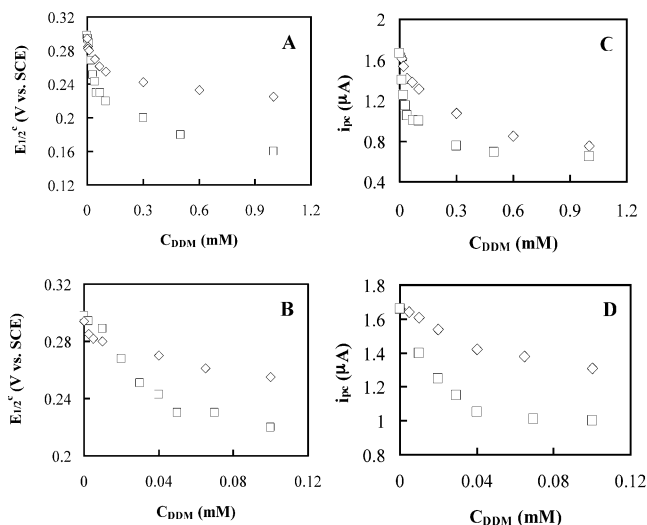


**Figure 2.**  $E_{1/2}^c$  (frames A and B) and  $i_{pc}$  (frames C and D) values as functions of the concentration of DDMs at a fixed  $[Ag^+] = 0.12$  mM. Squares, PAMAMG1NH<sub>2</sub>; diamonds, PAMAMG2OH. Scan rate  $v = 0.1$  V/s. Frames B and D are the expanded scales of frames A and frame C, respectively.

electrode and is stripped during reoxidation of Ag<sup>0</sup> upon scan reversal with an anodic peak potential,  $E_{pa}$  of +0.387 V. In the presence of 0.01 mM PAMAMG1NH<sub>2</sub>, with 0.12 mM Ag<sup>+</sup>,  $E_{pc} = +0.195$  V and  $E_{pa} = +0.349$  V vs SCE. Thus, both the  $E_{pc}$  and  $E_{pa}$  shift to more negative values as compared to a solution without PAMAMG1NH<sub>2</sub>. In this case, the  $E_{pc}$  and  $E_{pa}$  shifted to more negative potentials by 60 and 38 mV, respectively, indicating that PAMAMG1NH<sub>2</sub>-complexed Ag<sup>+</sup> is more difficult to reduce than uncomplexed Ag<sup>+</sup>, whereas complexed Ag<sup>0</sup> is easier to oxidize than bulk silver metal. Note that in the presence of DDM, the oxidation peak is characteristic of a solution species rather than a stripping peak, showing that Ag<sup>0</sup> does not form bulk metal on the electrode, but rather is present as a diffusing species in solution. In addition, the absence of any obvious Ag stripping peak suggests that at this ratio of analytical concentrations,  $C_{Ag^+}/C_{DDM} = 12$ , almost all of the Ag<sup>+</sup> is complexed.

Both the  $E_{pc}$  and  $E_{1/2}^c$  depended on the mole ratio of DDM to total Ag<sup>+</sup> concentration. Since  $E_{1/2}^c$ , as compared with  $E_{pc}$  in the present case, can be determined more easily and reliably, we summarize in Figure 2 the  $E_{1/2}^c$  values and the cathodic peak currents,  $i_{pc}$ , as functions of the concentration of DDMs at a fixed Ag<sup>+</sup> concentration of 0.12 mM. A limiting shift of  $\sim 0.16$  V in  $E_{1/2}^c$  was obtained for the Ag<sup>+</sup>-PAMAMG1NH<sub>2</sub> system at  $C_{DDM} = 1.5$  mM.

Reversibility of an electron-transfer reaction changed in the presence of a DDM. As shown in Figure 3, in a solution containing 0.12 mM Ag<sup>+</sup> and 0.1 mM PAMAMG1NH<sub>2</sub>, the  $E_{pc}$  shifts slightly to more negative values with increasing scan rate, while the  $E_{pa}$  was nearly independent of  $v$  in the range of  $5 < v < 500$  mV/s, indicating that the electron-transfer reactions are fast. For a Nernstian reaction,<sup>1a</sup>

$$i_{pc} = 2.69 \times 10^5 n^{3/2} AC_b^* D^{1/2} v^{1/2} \quad (1)$$

in which  $A$  is the surface area of the electrode,  $C_b^*$  is the bulk

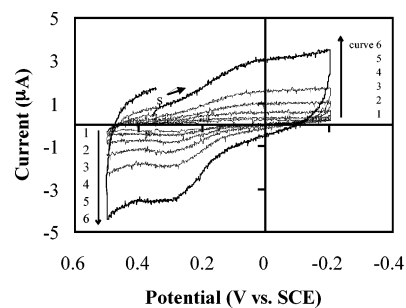


**Figure 3.** Scan rate dependence of CV for a solution containing 0.118 mM AgNO<sub>3</sub> and 0.12 mM PAMAMG1NH<sub>2</sub> in 0.2 M NaNO<sub>3</sub> at a 4-mm-diameter Au disk. Scan rate 10 (curve 1), 20 (curve 2), 50 (curve 3), 100 (curve 4), 200 (curve 5), and 500 mV/s (curve 6).

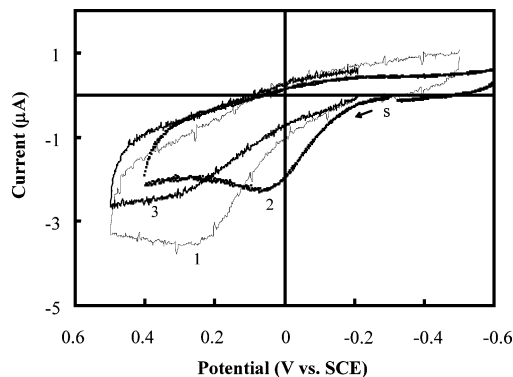


**Figure 4.** CVs in a 0.2 M NaNO<sub>3</sub> solution containing  $\sim 0.118$  mM Ag<sup>+</sup>-PAMAMG1NH<sub>2</sub> (0.118 mM AgNO<sub>3</sub> and 0.12 mM PAMAMG1NH<sub>2</sub>) after reduction of different concentrations of hydrazine. Curve 1, 0.05 mM hydrazine; curve 2, CV in 0.2 M NaNO<sub>3</sub> solution containing only 0.05 mM hydrazine; curve 3, 0.025 mM hydrazine with complex.

concentration of the metal complex, and the other quantities are previously defined. For a solution in which the ratio of DDM to Ag<sup>+</sup> was high, the  $i_{pc}$  was proportional to  $v^{1/2}$  (not shown) with a slope of the ( $i_{pc}$  vs  $v^{1/2}$ ) plot yielding a  $D$  value of  $9.1 \times 10^{-6}$  cm<sup>2</sup>/s for PAMAMG1NH<sub>2</sub>-complexed Ag<sup>+</sup>, assuming the reduction was a reversible, one electron-transfer process. As will be discussed later, an experiment on the titration of Ag<sup>+</sup> with PAMAMG1NH<sub>2</sub> DDM showed that a (1:1) (Ag<sup>+</sup>/PAMAMG1NH<sub>2</sub>) complex was the major silver species existing in such a solution. The 1:1 PAMAMG1NH<sub>2</sub>-complexed Ag<sup>+</sup> can be further transformed into DDM-bound zerovalent silver species by adding a suitable reducing agent. There are several frequently used reducing agents, such as borohydride, glucose, citrate, or hydrazine; however, significant rates of reduction of Ag<sup>+</sup> by citrate or glucose can only take place at elevated temperatures. To carry out the reduction at a reasonably high rate at room temperature with minimum amounts of unwanted products and large silver nanoparticles (not small clusters), hydrazine was used as the reducing agent. As shown in curve 3 of Figure 4, the addition of hydrazine ( $\leq 1/4$  of  $[Ag^+]$ ) into a 1:1 PAMAMG1NH<sub>2</sub>/Ag<sup>+</sup> solution reduced the complex partially, as shown by the enhanced oxidation current when the electrode potential was scanned positive from the initial rest potential ( $\sim -0.2$  V vs SCE). A broad current peak associated with a diffusion-limited electron transfer of a solution species, rather than a sharp stripping peak associated with a surface film, was obtained. Notice that this oxidation peak occurred at a potential more positive than that for hydrazine oxidation (curve 2, Figure

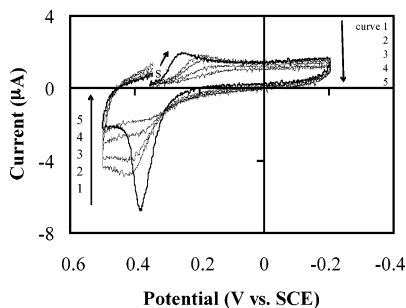


**Figure 5.** A series of CVs of 0.12 mM  $\text{Ag}^+$  in 0.2 M  $\text{NaNO}_3$  at an inlaid Au disk electrode (radius  $\sim 0.2$  cm) in the absence and presence of various PAMAMG2OH concentrations. Potential scan rate,  $\nu = 0.1$  V/s. Curve 1, no DDM; curve 2, 0.1 mM DDM; curve 3, 0.3 mM DDM; curve 4, 0.6 mM DDM; curve 5, 1.0 mM DDM.

4) but less positive than that for bulk silver oxidation. We attribute this peak to the oxidation of a zerovalent silver species. The formation of zerovalent silver species is confirmed by UV–vis spectra of the solution, as discussed later. The anodic peak current,  $i_{\text{pa}}$ , increased and the  $E_{\text{pa}}$  shifted to more negative values with an increasing concentration of hydrazine (e.g.,  $\sim 1/2$  of  $[\text{Ag}^+]$  for curve 1 of Figure 4) due to the formation of more  $\text{Ag}^0$  species and, finally, from a contribution for the oxidation of both  $\text{Ag}^0$  species and excess hydrazine.

**Chronoamperometry.** A typical current vs time ( $i$  vs  $t$ ) curve for a potential step (+0.35 to 0 V vs SCE) experiment at an Au disk (radius  $\sim 0.2$  cm) in a 0.2 M  $\text{NaNO}_3$  solution containing 0.12 mM  $\text{Ag}^+$  is shown in the Supporting Information section, Figure S1A. The corresponding  $i$  vs  $t^{-1/2}$  plot is shown in Figure S1B. The  $i$  vs  $t^{-1/2}$  plot showed good linearity over the time domain between 1 and 40 ms. A small offset of a few microamperes, associated with the small background current, was observed in the intercept of the linear fitting line. For a diffusion-limited electron-transfer reaction at a macrodisk electrode, the slope of the linear  $i$  vs  $t^{-1/2}$  plot is  $nFAC^*(D/\pi)^{1/4}$ ,<sup>1a</sup> where  $F$  is the Faraday constant and the other symbols are as defined previously. From the slope of the  $i$  vs  $t^{-1/2}$  plot, we determine a  $D$  value of  $1.5 \times 10^{-5}$   $\text{cm}^2/\text{s}$  for free  $\text{Ag}^+$ , with  $nC^* = 1.2 \times 10^{-7}$  mol/ $\text{cm}^3$ . This value agrees reasonably well with reported values.<sup>9</sup>

A similar potential step experiment was carried out at the same disk after the addition of 0.1 mM PAMAMG1NH<sub>2</sub> into the  $\text{Ag}^+$  solution. Good linearity with a nearly zero intercept of the corresponding  $i$  vs  $t^{-1/2}$  plot was also found over a time domain longer than 10 ms (Figure SI2). The slope of the  $i$  vs  $t^{-1/2}$  plot with  $nC^* = 1.2 \times 10^{-7}$  mol/ $\text{cm}^3$  yields a  $D$  value of  $8.3 \times 10^{-6}$   $\text{cm}^2/\text{s}$  for the silver–PAMAMG1NH<sub>2</sub> complex, that is,  $\sim 2/3$  that of uncomplexed  $\text{Ag}^+$  and slightly smaller than that determined from CV.

**Silver–PAMAMG2OH System, Cyclic Voltammetry.** Figure 5 shows a series of CVs of 0.12 mM  $\text{Ag}^+$  analogous to those in Figure 1, except in solutions containing various concentrations of PAMAMG2OH. As with  $\text{Ag}^+$ –PAMAMG1NH<sub>2</sub>, the addition of DDM into an  $\text{Ag}^+$  solution causes the  $E_{\text{pc}}$  to shift to more negative values. However, the limiting shift in  $E_{1/2}^c$  is smaller and estimated to be only  $\sim 0.065$  V (see Figure 2). Although significant

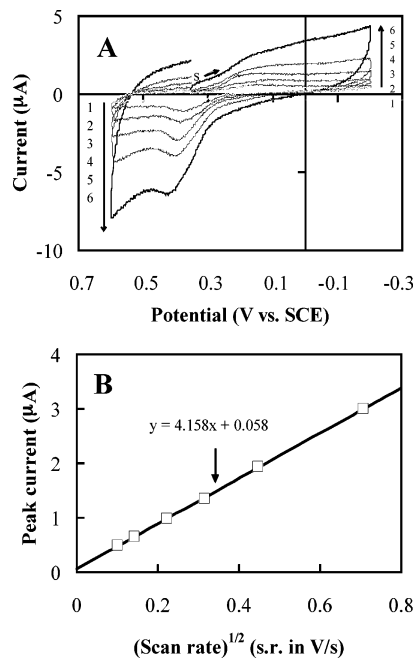


**Figure 6.** (A) Scan rate dependence of CV for a solution containing 0.118 mM  $\text{AgNO}_3$  and 0.12 mM PAMAMG1NH<sub>2</sub> in 0.2 M  $\text{NaNO}_3$  at a 4-mm-diameter Au disk. Scan rate: 10 (curve 1), 20 (curve 2), 50 (curve 3), 100 (curve 4), 200 (curve 5), and 500 mV/s (curve 6). (B) The corresponding scan rate dependence of  $i_{\text{pc}}$ .

reoxidation of complexed  $\text{Ag}^0$ , as compared with that of bulk silver metal, is observed at more negative potentials, the anodic current peaks are at more positive potentials, suggesting slower heterogeneous oxidation kinetics, as compared to the oxidation of bare silver.

As shown in Figure 6A, in a solution containing 0.12 mM  $\text{Ag}^+$  and 0.1 mM PAMAMG2OH, the  $E_{\text{pc}}$  was nearly independent of  $\nu$  in the range of  $5 < \nu < 500$  mV/s, while the  $E_{\text{pa}}$  shifted to more positive values with increasing  $\nu$ , indicating slow kinetics for oxidation. The reduction current,  $i_{\text{pc}}$  (taken at  $E = 0.2$  V), was proportional to  $\nu^{1/2}$  (see Figure 6B) and like the  $E_{\text{pc}}$ , depended on the concentration of DDM for a fixed total  $[\text{Ag}^+]$ . The  $i_{\text{pc}}$  as a function of the concentration of PAMAMG2OH at a fixed total  $[\text{Ag}^+] = 0.12$  mM is given in Figure 2.

**Chronoamperometry.** A potential step experiment was also carried out, as with the G1NH<sub>2</sub> DDM, on the silver–PAMAMG2OH system. The  $i$  vs  $t$  curve in a solution containing 0.12 mM  $\text{Ag}^+$  and 0.10 mM PAMAMG2OH is shown in the Supporting Information section, Figure SI3A. The linearity of the corresponding  $i$  vs  $t^{-1/2}$  plot was good over a reasonably wide time domain, as shown in Figure SI-3B. By taking  $nC^* = 1.2 \times 10^{-7}$  mol/ $\text{cm}^3$ , the slope of the  $i$  vs  $t^{-1/2}$  plot resulted in a  $D$  value of  $2.7 \times 10^{-6}$   $\text{cm}^2/\text{s}$  for this complex,  $1/5$ – $1/6$  that of uncomplexed  $\text{Ag}^+$ , consistent with the much higher molecular weight of the complex ( $\sim 32$  times), as compared with free  $\text{Ag}^+$ . The diffusion coefficients of  $\text{Ag}^+$  and 1:1  $\text{Ag}^+$ /PAMAM complexes obtained from chronoamperometry are summarized in Table 1.

**Ultraviolet–Visible Spectroscopic Measurements.** Comparison of the UV–vis spectra of various silver solutions with or without DDMs and before or after reduction clearly demonstrates the silver–DDM interaction. Figure 7A shows the UV–vis spectra of PAMAMG1NH<sub>2</sub> at different concentrations. The absorption

(9) (a) Meites, L. *J. Am. Chem. Soc.* **1951**, *73*, 395. (b) Meites, L. *J. Am. Chem. Soc.* **1951**, *73*, 1581. (c) West, P. W.; Dean, J.; Breda, E. J. *Collect. Czech. Chem. Commun.* **1948**, *13*, 1.

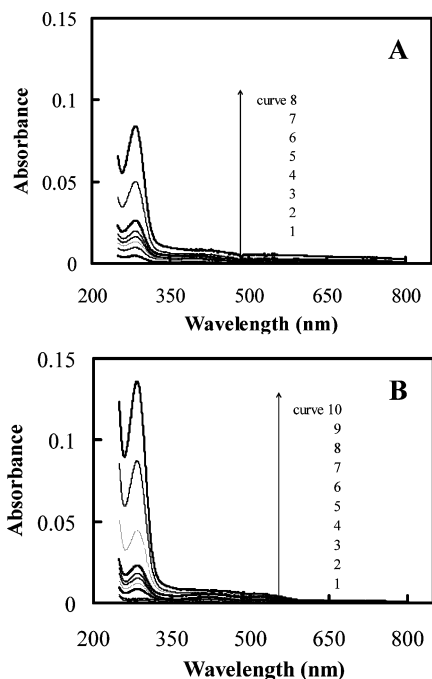


**Figure 7.** (A) UV-vis spectra of PAMAMG1NH<sub>2</sub> at different concentrations in water without Ag<sup>+</sup>: 0.01 (curve 1), 0.02 (curve 2), 0.03 (curve 3), 0.04 (curve 4), 0.05 (curve 5), 0.07 (curve 6), 0.1 (curve 7), and 0.3 mM (curve 8). (B) UV-vis spectra of PAMAMG1NH<sub>2</sub> at different concentrations in water with 0.12 mM Ag<sup>+</sup>: 0 (curve 1), 0.01 (curve 2), 0.02 (curve 3), 0.03 (curve 4), 0.04 (curve 5), 0.05 (curve 6), 0.07 (curve 7), 0.1 (curve 8), 0.3 (curve 9), and 0.5 mM (curve 10).

**Table 1. Diffusion Coefficients (*D*) and Molecular Weights (*MW*) of Ag<sup>+</sup> and 1:1 Ag<sup>+</sup>/PAMAM Complexes Obtained from Chronoamperometry**

compound	MW	normalized (MW) <sup>-1/2</sup>	<i>D</i> × 10 <sup>-6</sup> cm <sup>2</sup> /s
Ag <sup>+</sup>	108	5.6	15
Ag <sup>+</sup> -PAMAMG1NH <sub>2</sub>	1538	1.5	8.3
Ag <sup>+</sup> -PAMAMG2OH	3380	1	2.7

shows a peak at ~284 nm, and the peak absorbance is proportional to the concentration. Addition of 0.118 mM AgNO<sub>3</sub> to these DDM solutions causes the absorbance at 284 nm to decrease slightly (e.g., compare curve 8 of Figure 7B with curve 7 of Figure 7A for [PAMAMG1NH<sub>2</sub>] = 0.1 mM with or without 0.118 mM AgNO<sub>3</sub>, respectively), suggesting some interaction occurs between Ag<sup>+</sup> and DDM. No significant absorption was observed in the same wavelength region in a solution containing only 0.118 mM AgNO<sub>3</sub> (see curve 1 of Figure 7B), with no significant change in the shape of the spectra of DDM in the presence of 0.118 mM AgNO<sub>3</sub>. As shown in Figure 8, similar photometric behavior was observed for PAMAMG2OH DDM in the absence or presence of AgNO<sub>3</sub>. The absorbance at ~284 nm as a function of DDM concentration obtained from Figures 7 and 8A and B is summarized in Figure 8C. Both DDMs have rather small molar absorptivity,  $\epsilon$ , at ~284 nm ( $\epsilon = 280 \text{ M}^{-1} \text{ cm}^{-1}$  for PAMAMG1NH<sub>2</sub> and  $190 \text{ M}^{-1} \text{ cm}^{-1}$  for PAMAMG2OH).

After the addition of 0.03 mM hydrazine into a DDM-complexed silver solution containing 0.118 mM Ag<sup>+</sup> and 0.1 mM PAMAMG1NH<sub>2</sub>, a new shoulder (~345 nm) and a new peak

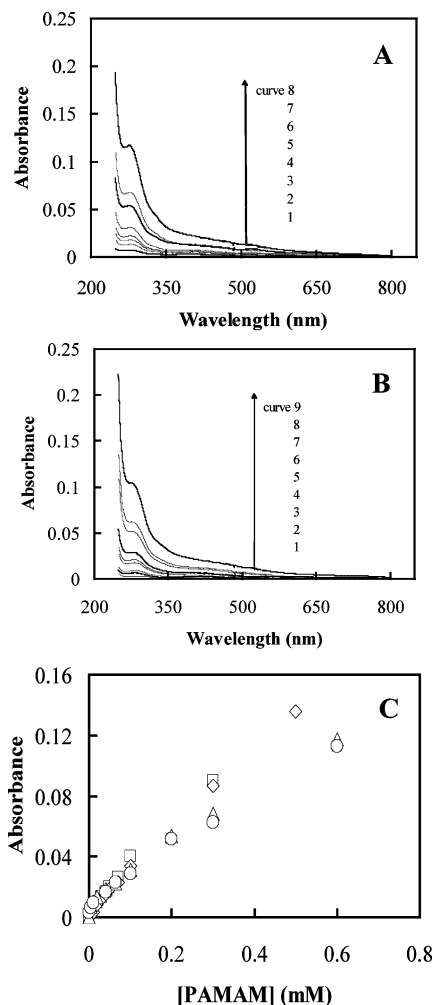


**Figure 8.** (A) UV-vis spectra of PAMAMG2OH at different concentrations in water without Ag<sup>+</sup>: 0.005 (curve 1), 0.02 (curve 2), 0.04 (curve 3), 0.0065 (curve 4), 0.1 (curve 5), 0.2 (curve 6), 0.3 (curve 7), and 0.6 mM (curve 8). (B) UV-vis spectra of PAMAMG1NH<sub>2</sub> at different concentrations in water with 0.12 mM Ag<sup>+</sup>: 0 (curve 1), 0.005 (curve 2), 0.01 (curve 3), 0.04 (curve 4), 0.065 (curve 5), 0.1 (curve 6), 0.2 (curve 7), 0.3 (curve 8), and 0.6 mM (curve 9). (C) Summary of the absorbance at ~284 nm as a function of DDM concentrations. Squares, PAMAMG1NH<sub>2</sub> only; diamonds, 0.12 mM AgNO<sub>3</sub> and varying [PAMAMG1NH<sub>2</sub>]; triangles, PAMAMG2OH only; and circles, 0.12 mM AgNO<sub>3</sub> and varying [PAMAMG2OH].

(~410 nm) developed due to the production of and absorption by silver nanoparticles. Note that the scale in Figure 9, curve 1 represents 10 times lower sensitivity than the other curves. Notice also that the absorbance at 284 nm was substantially enhanced, and the peak position was slightly blue-shifted. It merged into a strong absorption band at wavelengths shorter than 250 nm due to the formation of smaller silver clusters. The addition of hydrazine to a solution containing only DDM affects the spectrum in the visible region slightly (compare curve 3 with curve 2 of Figure 9). Similar behavior was observed for a DDM-complexed silver solution containing 0.118 mM Ag<sup>+</sup> and 0.1 mM PAMAMG2OH (not shown).

To minimize the agglomeration of silver clusters into larger nanoparticles during the reduction process, we used a lower concentration of Ag<sup>+</sup> and studied the concentration dependence of the growth rate of different zerovalent silver species upon reduction as shown by their different absorption peaks. As shown

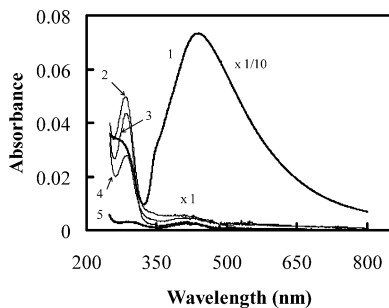


**Figure 9.** Change in UV–vis spectra of  $\text{Ag}^+$ –PAMAMG1NH<sub>2</sub> system after reduction: 0.118 mM  $\text{Ag}^+$  only (curve 5); 0.1 mM PAMAMG1NH<sub>2</sub> and 0.05 mM hydrazine (curve 3); 0.1 mM PAMAMG1NH<sub>2</sub> only (curve 2); 0.1 mM PAMAMG1NH<sub>2</sub> and 0.118 mM  $\text{AgNO}_3$  (curve 4); the above solution after reduction with 0.05 mM hydrazine (curve 1). Notice that the absorbance shown in curve 1 was reduced 10 times as compared to the other curves.

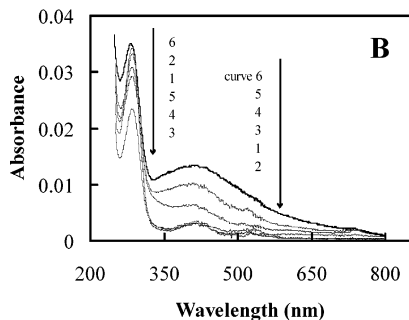
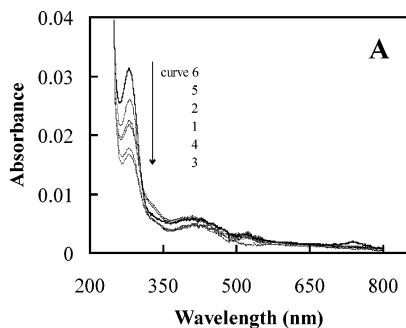


**Figure 10.** (A) UV–vis spectra of a solution containing 0.1 mM PAMAMG2OH with or without 0.024 mM  $\text{AgNO}_3$  added: curve 1, 0.1 mM PAMAMG2OH only; curve 2, 0.1 mM PAMAMG2OH with 0.1 mM hydrazine; curve 3, 0.024 mM  $\text{AgNO}_3$  and 0.1 mM PAMAMG2OH; curve 4, solution used in curve 3 after the addition of 0.003 mM hydrazine; curve 5, solution used in curve 3 after the addition of a total of 0.01 mM hydrazine; curve 6, solution used in curve 3 after the addition of a total of 0.02 mM hydrazine. (B) UV–vis spectra of a solution containing 0.1 mM PAMAMG1NH<sub>2</sub> with or without 0.024 mM  $\text{AgNO}_3$  added: curve 1, 0.1 mM PAMAMG1NH<sub>2</sub> only; curve 2, 0.1 mM PAMAMG1NH<sub>2</sub> with 0.06 mM hydrazine; curve 3, 0.024 mM  $\text{AgNO}_3$  and 0.1 mM PAMAMG1NH<sub>2</sub>; curve 4, solution used in curve 3 after the addition of 0.0033 mM hydrazine; curve 5, solution used in curve 3 after the addition of a total of 0.0066 mM hydrazine; curve 6, solution used in curve 3 after the addition of a total of 0.01 mM hydrazine.

in Figure 10A for a solution initially containing 0.1 mM PAMAMG2OH, the absorbance at the peak of  $\sim 284$  nm is nearly proportional to the concentration of added hydrazine, whereas that at  $\sim 410$  nm is nearly independent of the amount of hydrazine added into the solution. The enhancement of the absorbance at  $\lambda \leq 284$  nm, after the reduction process, is mainly associated with the formation of small silver clusters of less than 10 silver atoms,<sup>8</sup>

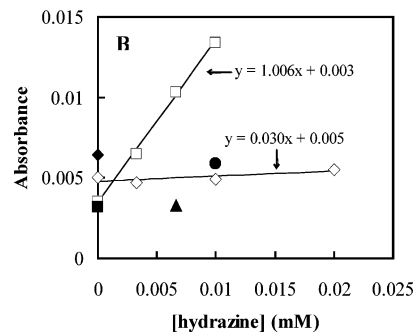
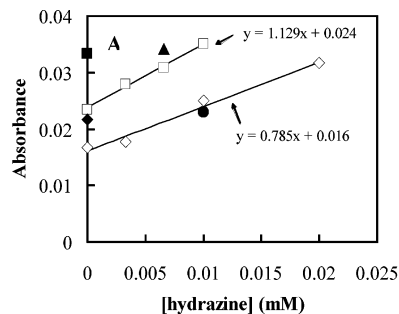


**Figure 11.** Absorbance of various solutions as functions of hydrazine concentration at  $\lambda_{\text{max}} \sim 283$  nm (A) and  $\sim 410$  nm (B). Open squares, 0.1 mM PAMAMG1NH<sub>2</sub> and 0.024 mM  $\text{Ag}^+$ ; open diamonds, 0.1 mM PAMAMG2OH and 0.024 mM  $\text{Ag}^+$ ; solid squares and solid triangle, 0.1 mM PAMAM only; solid diamonds and solid circle, 0.1 mM PAMAMG2OH only.

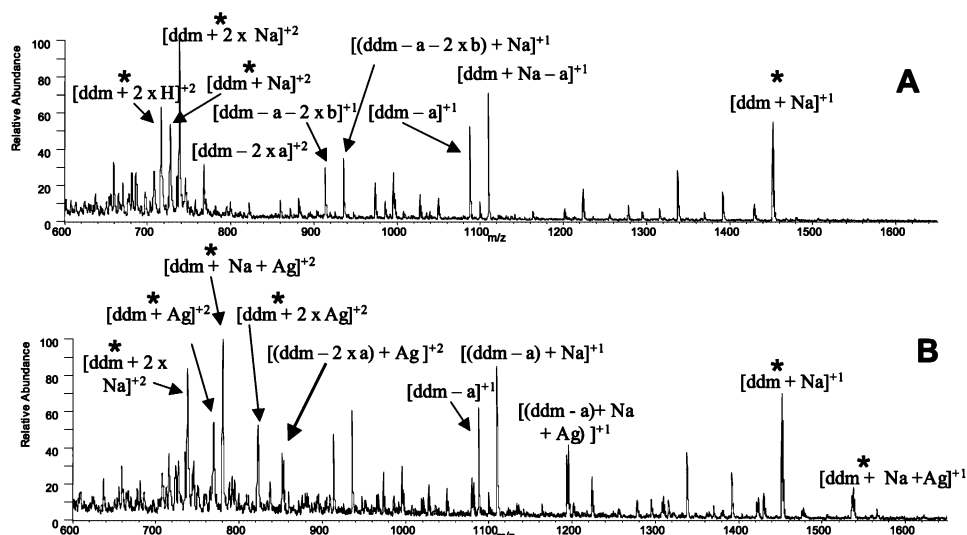
and the absorption at  $\sim 410$  nm is due to Mie surface plasma resonance (SPR)<sup>10</sup> of larger silver nanoparticles. These spectrophotometric results suggest that the reduction of the  $\text{Ag}^+$ –PAMAMG2OH complex favors the formation of small clusters, as compared to the growth of bigger nanoparticles.

Figure 10B shows the results of spectrophotometric titration of a solution containing 0.1 mM PAMAMG1NH<sub>2</sub>. As summarized in Figure 11, the absorbance at peaks near to 284 and 410 nm are both proportional to the concentration of hydrazine added and increase at a similar rate, suggesting that at least two differently sized zerovalent silver species grow in a similar pattern. These results are consistent with those observed previously for the  $\text{Cu}^{2+}$ –DDM systems,<sup>11</sup> suggesting that PAMAMG2OH (OH-terminated) favors the formation of intra-DDM silver clusters, whereas PAMAMG1NH<sub>2</sub> allows for the formations of both interior- and exterior-DDM zerovalent silver species. The latter was less stable and could further cause the agglomeration of silver clusters to form larger nanoparticles, as manifested by the observation of the SPR peak near 410 nm.

**Mass Spectrometric Measurement.** To learn more about the stoichiometry of the silver–DDM complexes, we carried out electrospray ionization mass spectrometry (ESI-MS) studies of the  $\text{Ag}^+$ –PAMAMG1NH<sub>2</sub> system. Solutions were prepared in water/methanol mixed solvents to enhance the ion abundance and signal-to-noise ratio. The spectra are fairly complicated, but most of the major peaks can be assigned on the basis of the  $m/z$  values and collisional activated dissociation (CAD)<sup>12</sup> fragmentation patterns. Figure 12A shows the ESI mass spectrum of PAMAMG1NH<sub>2</sub>

(10) Kreibig, U. In *Handbook of Optical Properties*; Hummel, R. E., Wibmann, P., Eds.; CRC Press: Boca Raton, FL, 1997; Vol. II, Chapter 7.

(11) Zhao, M.; Sun, L.; Crooks, R. M. *J. Am. Chem. Soc.* **1998**, *120*, 4877–4878.



**Figure 12.** SI Quadrupole ion trap mass spectra of solutions containing 10  $\mu\text{M}$  PAMAMG1NH<sub>2</sub> (abbreviated by DDM) alone (A), and 10  $\mu\text{M}$  AgNO<sub>3</sub> and 10  $\mu\text{M}$  PAMAMG1NH<sub>2</sub> (B) in 3:1 methanol/water mixed solvent. Peaks labeled with an asterisk (\*) correspond to complexes containing the intact dendrimer.

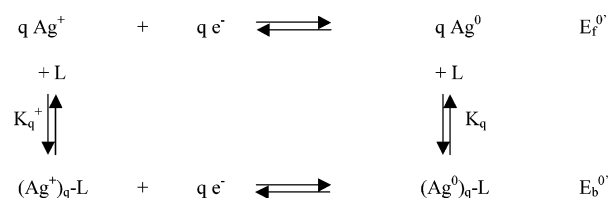
prepared in a 3:1 methanol/water (volume/volume) mixed solvent. A series of prominent peaks are assigned to the multiply charged molecular ions of protonated PAMAMG1NH<sub>2</sub> or ions complexed with Na<sup>+</sup>. The main source of the Na<sup>+</sup> contamination is the glass apparatus used in the syntheses of DDM and the glass containers used for storage of the solution. Some of the peaks interspersed between the molecular ion peaks correspond to DDMs containing defects, such as missing branches.<sup>1c</sup> For example, a peak at  $m/z$  1109.9 is associated with a Na<sup>+</sup> complex of the parent DDM with the loss of one amidoamine branch of mass 343.3 Da, and another peak at  $m/z$  768.0 is associated with a Na<sup>+</sup> complex of the DDM after loss of two amidoamine branches.

Figure 12B shows the mass spectrum of complexes of PAMAMG1NH<sub>2</sub> with silver(I) prepared by mixing equimolar (10  $\mu\text{M}$  each) Ag<sup>+</sup> and DDM in 3:1 methanol/water. The binding stoichiometries of 1:1 (Ag<sup>+</sup>/PAMAMG1NH<sub>2</sub>) (peaks at  $m/z$  769.3 for HAgDDM<sup>2+</sup>, 780.8 for NaAgDDM<sup>2+</sup>, 1537.8 for AgDDM<sup>+</sup>), were dominant for complexes observed under these conditions. A significant amount of the complex with a 2:1 (Ag<sup>+</sup>/PAMAMG1NH<sub>2</sub>) ratio ( $m/z$  822.8) also existed in the solution. The single-branch DDM defect ( $m/z$  1109.9 for its Na<sup>+</sup> complex as mentioned above) formed complexes with Ag<sup>+</sup> to yield a significant amount of a singly charged Ag<sup>+</sup> complex of 1:1 ratio ( $m/z$  1195.7), and the two-branch DDM defect ( $m/z$  768.0) complexes with Ag<sup>+</sup> to yield a singly charged complex of 1:1 ratio ( $m/z$  851.6).

## DISCUSSION

For a Nernstian electron-transfer reaction in which the oxidized and reduced forms associated with a complexation agent in solution, a square scheme (as shown below) can be applied for a single stoichiometric complex system. For the case presented in Scheme 1, L = DDM. Here,  $E_f^{0'}$  and  $E_b^{0'}$  are the formal potentials of the Ag<sup>+</sup>/Ag<sup>0</sup> couple in the free and complexed forms, respectively, and  $q$  is the number of Ag<sup>+</sup> complexed with one DDM

### Scheme 1



molecule. For simplicity, we assume that  $q$  values for DDM complexed silver ion and zerovalent silver species are identical, at least in the initial stage of the reduction process.  $K_q^+$  and  $K_q$  are the microscopic formal equilibrium constants for complexation of Ag<sup>+</sup> and Ag<sup>0</sup> species to DDM and are expressed as follows.

$$K_q^+ = [\text{Ag}_q\text{L}^{q+}] / ([\text{Ag}^+]^q[\text{L}]); \quad K_q = [\text{Ag}_q\text{L}] / (a_{\text{Ag}^0}^q[\text{L}]) \quad (2)$$

in which  $[\text{Ag}_q\text{L}^{q+}]$  and  $[\text{Ag}^+]$  represent the equilibrium concentrations of the Ag<sup>+</sup>-DDM complex and free Ag<sup>+</sup>,  $[\text{Ag}_q\text{L}]$  and  $[a_{\text{Ag}^0}]$  are the corresponding concentrations of the Ag<sup>0</sup>-DDM complex and the activity of free Ag<sup>0</sup>, and  $C_s$  is the concentration of free DDM ligand.

At 25 °C and assuming that  $n = 1$  and  $q = 1$ , we have<sup>1a</sup>

$$E_f = E_f^{0'} + 0.059 \log([\text{Ag}^+] / a_{\text{Ag}^0}) \quad (3)$$

$$E_b = E_b^{0'} + 0.059 \log([\text{AgL}^+] / [\text{AgL}]) \quad (4)$$

At equilibrium, one can obtain the relation shown below from eqs 2-4.

$$E_b^{0'} - E_f^{0'} = 0.059 \log(K^0 / K_1^+) \quad (5)$$

Thus, from the CV, a limiting shift of 0.16 V in  $E_{1/2}^c$  for the Ag<sup>+</sup>-PAMAMG1NH<sub>2</sub> complex yields a  $K_1^+ / K_1$  of 515 for the Ag<sup>+</sup>-PAMAMG2OH complex and a limiting shift of 0.065 V,  $K_1^+ / K_1 =$

(12) Busch, K. L.; Glish, G. L.; McLuckey, S. A. *Mass Spectrometry/Mass Spectrometry: Techniques and Applications of Tandem Mass Spectrometry*; VCH Publishers: New York, 1988.

13. These results indicate that DDM binds more strongly to  $\text{Ag}^+$  than it does to zerovalent silver and also suggests that the silver species interacts with DDM predominantly via amine groups, especially those periphery primary amine groups in the amine-terminated DDM. This is consistent with the  $K_q^+$  values determined from the voltammetric titrations discussed below.

This square scheme has been utilized to probe the interaction of metal complexes with DNA<sup>13</sup> and to examine electron-transfer reactions associated with host-guest complexation<sup>14</sup> on the basis of voltammetric measurements. Under the assumption of diffusion-controlled electron transfer, two limiting cases hold for the current in voltammetric measurements, depending on whether the interconversion of free and complexed  $\text{Ag}^+$ , in Scheme 1, is treated as static (no interconversion takes place during the time of the normal CV experiment, eq 6) or mobile (rapid interconversion during a scan, eq 7).<sup>13,15</sup>

$$i_{pc} = BC_t^+ [D_f^{1/2} + (D_b^{1/2} - D_f^{1/2})x_b^+] \quad (6)$$

$$i_{pc} = BC_t^+ [D_f + (D_b - D_f)x_b^+]^{1/2} \quad (7)$$

In which  $B = 2.69 \times 10^5 n^{3/2} A v^{1/2}$  for a Nernstian reaction, which represents the appropriate concentration-independent terms in the voltammetric expression.  $D_f$  and  $D_b$  are the diffusion coefficients of free and complexed  $\text{Ag}^+$ , respectively,  $x_b^+$  is the mole ratio of the complexed  $\text{Ag}^+$ , and  $C_t^+$  is the analytical concentration of  $\text{Ag}(\text{I})$ , that is,

$$x_b^+ = q[\text{Ag}_q\text{L}^{q+}]/C_t^+ \quad (8)$$

$$C_t^+ = [\text{Ag}^+] + q[\text{Ag}_q\text{L}^{q+}] \quad (9)$$

Normalizing  $i_{pc}$  in eqs 6 and 7 with the  $i_{pc}$  value at  $x_b^+ = 0$ , that is,  $BC_t^+ D_f^{1/2}$  and with some mathematical manipulation, yields expressions in terms of a dimensionless parameter,  $I_{pc}$ ,

$$I_{pc} = 1 + [(D_b/D_f)^{1/2} - 1]x_b^+ \quad \text{for the static case} \quad (10)$$

$$I_{pc}^2 = 1 + [(D_b/D_f) - 1]x_b^+ \quad \text{for the mobile case} \quad (11)$$

where  $I_{pc} = i_{pc}/BC_t^+ D_f^{1/2}$ .

Taking  $R^+ = C_s^*/C_t^+$  for total  $\text{Ag}^+$  species, in which  $C_s^*$  is the total concentration of DDM, we obtain eq 12 for  $R^+$  as a function of  $x_b^+$ ,  $K_q^+$ ,  $C_t^+$  and  $q$ .

$$R^+ = x_b^+ \{1 + [1/(K_q^+(C_t^+)^q(1 - x_b^+)^q)]\} \quad (12)$$

The variation of  $x_b^+$  with  $R^+$  over a wide range of  $K_q^+$  at constant  $C_t^+$  is shown in Figure 13, and the voltammetric behavior, in terms of  $I_{pc}$  or  $I_{pc}^2$  vs  $x_b^+$  for the static and mobile case is shown in Figure 14. The four curves in Figure 13A represent different complexation constants,  $K_q^+$ , of  $1.0 \times 10^5$ ,  $1.0$

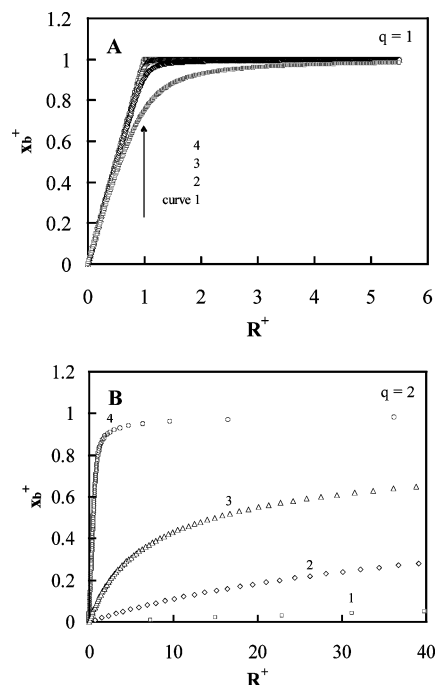


**Figure 13.** Molar fraction of complexed  $\text{Ag}^+$  as a function of  $R^+$  at  $C_t^+ = 1.18 \times 10^{-4}$  M for different  $K_q^+$  values;  $q = 1$  (frame A) and  $q = 2$  (frame B). Curve 1,  $K_q^+ = 1.0 \times 10^5$ ; curve 2,  $K_q^+ = 1.0 \times 10^6$ ; curve 3,  $K_q^+ = 1.0 \times 10^7$ ; curve 4,  $K_q^+ = 5.0 \times 10^9$ . The unit is in  $\text{M}^{-1}$  for  $q = 1$  and  $\text{M}^{-2}$  for  $q = 2$ .

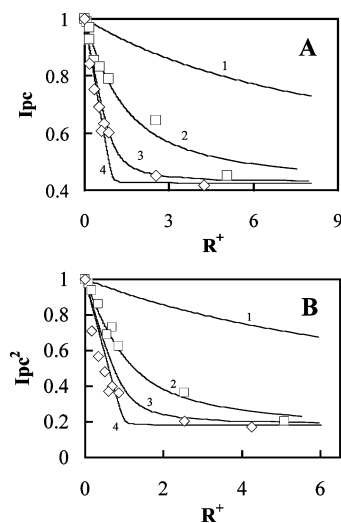


**Figure 14.** A series of theoretical curves of  $I_{pc}$  (frame A) and  $I_{pc}^2$  (frame B) vs  $R^+$  based on eqs 10, 11, and 12 for different  $K_q^+$  values. In the calculation, we take  $C_t^+ = 0.12$  mM and  $q = 1$  as  $R^+ > 1$  and  $q = 2$  as  $R^+ < 1$ , and  $D_b/D_f = 0.18$  and  $0.55$ , as determined from chronoamperometry, for  $\text{Ag}^+$ -PAMAMG1NH<sub>2</sub> and  $\text{Ag}^+$ -PAMAMG1OH systems, respectively. Lines are theoretical curves:  $K_q^+ = 1.0 \times 10^6$  (curve 1),  $1.1 \times 10^7$  (curve 2),  $1.0 \times 10^8$  (curve 3), and  $4.0 \times 10^9$   $\text{M}^{-1}$  (curve 4) for  $q = 1$ , and  $1.0 \times 10^6$  (curve 1),  $2.0 \times 10^7$  (curve 2),  $1.0 \times 10^8$  (curve 3),  $5.0 \times 10^9$   $\text{M}^{-2}$  (curve 4) for  $q = 2$ . Symbols are experimental data: squares ( $\text{Ag}$ -PAMAMG1NH<sub>2</sub> system), diamonds ( $\text{Ag}$ -PAMAMG2OH system).

$\times 10^6$ ,  $1.0 \times 10^7$ , and  $5.0 \times 10^9$   $\text{M}^{-1}$ , respectively, with  $C_t^+ = 0.12$  mM and  $q = 1$ . The steepness of the initial rise in  $x_b^+$  with increasing  $R^+$  increases as  $K_q^+$  becomes larger. At the lowest  $K_q^+$  value considered here, that is,  $1.0 \times 10^5$   $\text{M}^{-1}$  (solid squares curve),  $x_b^+$  can reach 0.8 at  $R^+ = 1$  and approaches unity when  $R^+$

(13) Carter, M. T.; Rodriguez, M.; Bard, A. J. *J. Am. Chem. Soc.* **1989**, *111*, 8901.

(14) (a) Matsue, T.; Evans, D. H.; Osa, T.; Kobayashi, N. *J. Am. Chem. Soc.* **1985**, *107*, 341. (b) Rusling, J. F.; Shi, C.-N.; Kumosinski, T. F. *Anal. Chem.* **1988**, *60*, 1260. (c) Zana, R.; Mackay, R. A. *Langmuir* **1986**, *2*, 109.

(15) Evans, D. H. *J. Electroanal. Chem.* **1989**, *258*, 451.

is  $>5$ . At  $K_q^+$  values higher than  $1.0 \times 10^7 \text{ M}^{-1}$ , almost all ( $>98\%$ ) of the  $\text{Ag}^+$  species are in the complexed form at  $R^+ = 1$ . Thus, under such conditions frequently used in our EC and spectroscopic experiments (i.e.,  $[\text{Ag}^+] = 0.12 \text{ mM}$  and  $[\text{DDM}] = 0.1 \text{ mM}$ ), most of the  $\text{Ag}^+$  species in the solution are complexed. When  $K_q^+$  is large, a significant change in  $x_b^+$  with increasing  $R^+$  occurs at  $R^+$  near 1, and little change occurs at larger  $R^+$ . This is consistent with the observation that both  $i_{pc}$  and  $E_{1/2}^c$  change significantly at  $R^+ < 1$  and much less at  $R^+ > 1$ . As shown in Figure 13B, when  $q = 2$ , the initial rise in  $x_b^+$  with increasing  $R^+$  becomes less steep, as compared to the case of  $q = 1$ , at the same value of  $K_q^+$ . The end point of the titration curve becomes more difficult to define. At  $K_q^+$  of  $< 10^5 \text{ M}^{-2}$ , the curve is barely distinguishable from a straight line nearly parallel to the  $R^+$  axis (see solid squares in Figure 13B).

Figure 14 shows a series of theoretical curves of  $I_{pc}$  and  $I_{pc}^2$  vs  $R^+$  based on eqs 10, 11, and 12 for different  $K_q^+$  values. In the calculation, we take  $C_t^+ = 0.12 \text{ mM}$  and  $q = 1$  at  $R^+ > 1$  and  $q = 2$  at  $R^+ < 1$ , and  $D_b/D_f = 0.18$  and  $0.55$ , as determined from chronoamperometry, for  $\text{Ag}^+$ -PAMAMG1NH<sub>2</sub> and  $\text{Ag}^+$ -PAMAMG1OH systems, respectively. The fit of the theoretical curves to the experimental data can be achieved at  $R^+ > 1$  and gives  $K_1^+ = 4.0 \times 10^9 \text{ M}^{-1}$  for the 1:1  $\text{Ag}^+$ /PAMAMG1NH<sub>2</sub> complex and  $K_1^+ = 1.1 \times 10^7 \text{ M}^{-1}$  for the 1:1  $\text{Ag}^+$ /PAMAMG2OH complex. The latter is comparable to  $K_1^+$  for the diamine complex of  $\text{Ag}^+$  and ammonia.<sup>16</sup> This voltammetric titration result, that is, the formation of a 1:1 complex as the major silver-containing species for the  $\text{Ag}^+$ -PAMAMG1NH<sub>2</sub> system with equimolar  $\text{Ag}^+$  and DDM, is consistent with the finding obtained from the MS measurements. Notice that as indicated by the results of the voltammetric titration,  $\text{Ag}^+$  binds more strongly with the amine-terminated DDM, as compared with the hydroxyl-terminated DDM of the same generation. At  $R^+ < 1$ , the experimental  $I_{pc}$  and  $I_{pc}^2$  data deviate substantially from the theoretical curves if the same set of parameters is used. A better fit can be achieved in this domain by assuming  $q \geq 2$  with comparable  $K_2^+$  values. However, one has to realize that mixed stoichiometric silver complexes very likely coexist in this domain, and a more complicated reaction scheme is required for data analyses.

It is worthwhile to examine the behavior of the two limiting models, eqs 10 and 11. In the limit of no interconversion of free and complexed  $\text{Ag}^+$ , on the time scale of the normal CV experiment, for example,  $v = 0.1 \text{ V/s}$ , the total current measured is always smaller than in the case of rapid interconversion when  $R^+$  is  $>0$ . Thus, the assumption of rapid interconversion will yield  $K_q^+$  values that are larger than those given by the static model with the same diffusion coefficients and  $q$  values. For our systems, the  $K_1^+$  values obtained from the two limiting models differ by no more than a factor of 1.8 because the  $K_1^+$  values are large, leading to a small contribution of the total current from free  $\text{Ag}^+$ . Within experimental error, it is difficult to determine which model is more appropriate to use for the determination of  $K_q^+$  and  $q$ . We summarize the results in Table 2 on the basis of the calculation obtained from the static model, since it gives a slightly better fit of the theoretical curves to the experimental results with the same

**Table 2. Stability Constants ( $K_q^+$ ) and  $q$  Values of  $\text{Ag}^+$  and PAMAM Complexes**

ligand	$q$	$K_q^+$
PAMAMG1NH <sub>2</sub>	1	$4.0 \times 10^9 \text{ M}^{-1}$
PAMAMG2OH	1	$1.1 \times 10^7 \text{ M}^{-1}$
PAMAMG1NH <sub>2</sub>	2	$5.0 \times 10^9 \text{ M}^{-2}$
PAMAMG2OH	2	$2.0 \times 10^7 \text{ M}^{-2}$

<sup>a</sup> As  $R^+ < 1$ , better fit is obtained by assuming  $q \geq 2$ , and  $K_q^+$  now is in  $\text{M}^{-2}$ .

set of parameters (see Figure 14), although both models can give a good fit if different  $K_1^+$  values for different models are used.

In the UV-vis spectrophotometric measurements of reduced PAMAMG2OH-hosted silver species at low concentration (see Figures 10A and 11), the lack of absorbance near 410 nm, which is characteristic of Mie SPR for silver nanoparticles, indicates that zerovalent silver clusters rather than larger nanoparticles are produced under the conditions used. As the  $K_q^+$  value indicates, the surface hydroxyl groups do not bind  $\text{Ag}^+$  as strongly as surface amine groups. Thus, OH-terminated DDM favors the formation of an intradendrimer  $\text{Ag}^+$  complex through interior tertiary amine groups, and interior-DDM silver clusters can be formed after reduction. As opposed to  $\text{Ag(I)}$  reduction in PAMAMG2OH, the results for PAMAMG1NH<sub>2</sub>, as shown in Figures 10B and 11, show that both small clusters and larger nanoparticles are formed at the same concentration of the  $\text{Ag}^+$ -PAMAMG1NH<sub>2</sub> complex an hour after reduction, although long-term stabilities and the growth kinetics of the clusters or nanoparticles have not been carried out. These results are consistent with the conclusion drawn from the voltammetric titration by considering that amine-terminated DDM, as compared with hydroxyl-terminated DDM, favors the formation of exterior-DDM silver clusters after reduction, which can lead to agglomeration of the Ag clusters to form larger nanoparticles.

A photometric titration is, in general, useful for the determination of the stability constant of a complex.<sup>17</sup> However, the end point of the photometric titration curve, as shown in Figure 8C, is difficult to define because there are no dramatic changes either in the shape of the spectra or in the absorbance at peak 284 nm for the  $\text{Ag}^+$ -PAMAM systems studied here. The curves are barely distinguishable from straight lines at high  $R^+$  values, although more significant curvature is observed at low  $R^+$ .

## CONCLUSIONS

Electrochemical methods, complementary to spectroscopic and mass spectrometric techniques, have been used to probe the complexation of silver with low-generation amine- or hydroxyl-terminated PAMAM dendrimers. Stability constants and the stoichiometry of the complexes can be obtained from the dependence of peak current on  $R^+$  from the voltammetric titration experiments. The stoichiometry of the complexes obtained from the EC method agrees well with that obtained from mass spectrometry.  $\text{Ag}^+$  binds more strongly with amine-terminated

(16) Shumilova, N. A.; Zhutava, G. V. In *Encyclopedia of Electrochemistry of the Elements*; Bard, A. J., Ed.; Marcel Dekker: New York, 1978; Vol. VIII, p 32.

(17) (a) Rossotti, F. J. C.; Rossotti, H. *The Determination of Stability Constants*, McGraw-Hill: New York, 1961. (b) Ramette, R. W. *J. Chem. Educ.* **1967**, *44*, 647.

G1PAMAM than with hydroxyl-terminated G2PAMAM.  $E^0$  of the Ag–PAMAMG1NH<sub>2</sub><sup>+ / 0</sup> couple (estimated from the average of  $E_{pc}$  and  $E_{pa}$ ) shifted to more negative values than that of Ag<sup>+ / 0</sup>. Spectroscopic results suggest that the OH-terminated G2PAMAM favors the formation of small zerovalent silver clusters after reduction, whereas with amine-terminated G1PAMAM, both clusters and larger nanoparticles are formed simultaneously under similar conditions. This might be attributed to the formation of an exterior Ag<sup>+</sup>–DDM complex for amine-terminated DDM, as compared to the formation of an interior Ag<sup>+</sup>–DDM complex for OH-terminated DDM prior to the reduction process. The present results also suggest that nucleation and growth are important during the reduction process, since clusters or nanoparticles can be produced from a 1:1 Ag<sup>+</sup>–DDM complex precursor.

#### ACKNOWLEDGMENT

We acknowledge support of this research from Nucrust Pharmaceuticals and the Welch Foundation (F-1155).

#### SUPPORTING INFORMATION AVAILABLE

Typical current vs time  $i$  vs  $t$  curve for the potential step (+0.35 to 0 V vs SCE) experiment at an Au disk (radius ~0.2 cm) in a 0.2 M NaNO<sub>3</sub> solution containing 0.12 mM Ag<sup>+</sup>, a solution containing 0.12 mM Ag<sup>+</sup> and 0.1 mM PAMAMG1NH<sub>2</sub>, and a solution containing 0.12 mM Ag<sup>+</sup> and 0.1 mM PAMAMG2OH. This material is available free of charge via the Internet at <http://pubs.acs.org>.

Received for review December 17, 2004. Accepted April 26, 2005.

AC048133G